Can the Insect Path Integration Memory be a Bump Attractor?

Ioannis Pisokas[1*] and Matthias H. Hennig[1]

[1]School of Informatics, University of Edinburgh, United Kingdom

Abstract

Many animal species are able to return to their nest after a foraging excursion without using familiar visual cues to guide them. They accomplish this by using a navigation competence known as path integration, which is vital in environments that do not have prominent visual features. To perform path integration, an animal maintains an estimate of the distance and direction to its origin as it moves. The distance and direction information needs to be maintained in memory for the duration of the trip so that the animal can return to its nest. However, the neural substrate of this memory remains unclear. A common hypothesis is that the information is maintained in a bump attractor's state. We test the bump attractor hypothesis and find that its predictions do not match behavioural data from ants, thus falsifying the bump attractor hypothesis and raising the need for alternative models of path integration memory.

1 Introduction

When a foraging ant of the species *Cataglyphis fortis*, inhabiting the Saharan desert, embarks in search of food, it typically follows a circuitous path. However, once it finds a food item, it readily returns to its nest, travelling along a straight path, even though there are no visual cues to guide its trip (Müller and Wehner, 1988; Collett, 2019; Menzel and Muller, 1996). To do this, the animal maintains at all times an estimate of its relative position in respect to its origin, using a navigational competence known as 'path integration' or 'dead-reckoning' (Darwin, 1873; von Frisch, 1967; Mittelstaedt and Mittelstaedt, 1980; Müller and Wehner, 1988). This relative position estimate is believed to be maintained by continuously updating a vectorial representation pointing to its origin as it moves in its environment (Heinze et al., 2018; Collett, 2019). This vectorial representation is commonly referred to as a 'home vector'[1] (Collett, 2019).

To update its home vector, the insect has to have access to two pieces of information at every instant in time, its current heading and an estimate of the distance it has travelled along this direction. These displacement estimates are accumulated continuously updating the home vector (Heinze et al., 2018; Collett, 2019). This procedure is similar to that employed by sea navigators in the past who used a magnetic compass to gauge their heading and vector addition to track their position on a map.

Path integration has been described in several species, including desert ants of the genus *Cataglyphis*, the honey bee *Apis mellifera*, the sweat bee *Megalopta genalis*, the fruit fly *Drosophila melanogaster*, as well as in rodents (Müller and Wehner, 1988; Collett, 2019; Menzel and Muller, 1996; Heinze and Homberg, 2007; Heinze et al., 2013; Stone et al., 2017; Kim and Dickinson, 2017; McNaughton et al., 2006). The spatial scale of path integration varies between species. For instance, fruit flies

[1]The home vector is a conceptual vector with direction parallel to the line connecting the current animal location and its nest and length corresponding to the current distance of the animal from its nest.

(*Drosophila melanogaster*) employ path integration for returning to a previously visited drop of sugar a few centimetres away (Kim and Dickinson, 2017), while other insect species use path integration to return to their nest over much larger distances, for instance, hundreds of meters in the case of the desert ant *Cataglyphis fortis*, or several kilometres in the case of the honey bee *Apis mellifera* (Sommer and Wehner, 2004; Cheng et al., 2005; Huber and Knaden, 2015).

At the end of its excursion, a path integrating animal can return to its nest by travelling in the direction and for the distance indicated by its accumulated home vector (Müller and Wehner, 1988; Menzel and Muller, 1996; Collett, 2019). To do this, the animal needs to be able to maintain its home vector in memory for the duration of its excursion, even if it is interrupted and prohibited from returning to its nest for several hours (Ziegler and Wehner, 1997; Cheng et al., 2005). Therefore, a memory mechanism that can be updated quickly and maintain its state long enough is required. However, the substrate of the employed memory remains unknown.

Most path integration models leave the memory substrate unspecified, while some authors have suggested that the home vector memory might be maintained through reverberating neural activity and more specifically, in a bump attractor network (McNaughton et al., 1996; Samsonovich and McNaughton, 1997; Conklin and Eliasmith, 2005; McNaughton et al., 2006; Burak and Fiete, 2009; Vickerstaff and Di Paolo, 2005; Haferlach et al., 2007; Kim and Lee, 2011; Goldschmidt et al., 2015; Webb and Wystrach, 2016; Stone et al., 2017; Goldschmidt et al., 2017).

Bump attractors are recurrent neural networks that maintain a localised peak of neural activity. A bump attractor can be used to encode an agent's spatial position as the location of the peak of neural activity ('activity bump') in the network (Fig 1A). If we imagine that the neurons of the bump attractor are organised topologically (if not spatially) on a line, the higher the represented spatial value, the further along the line the most active neurons will be located (Fig 1A). This constitutes a positional encoding of value along a line of neurons.

In bump attractor networks, the activity bump is maintained through specific synaptic connectivity with short-range excitation and long-range inhibition (Fig 1B). The location of the activity bump can be changed by an external input that breaks the balance between excitation and inhibition to move the bump towards a particular direction. With appropriate connectivity, the amount of the bump's movement along the neural network can be proportional to the integral of the input stimulus over time (Skaggs et al., 1995). In this case, bump attractor networks can be used as neural integrators that encode the integral of the input signal as the location of the activity bump along the network.

Bump attractor networks have been used to model systems that gradually accumulate velocity signals, such as angular velocity for tracking the head direction of rodents (Zhang, 1996; Redish et al., 1996; Goodridge and Touretzky, 2000; Boucheny et al., 2005) or translational velocity in path integration models of rodent place and grid cells to track the spatial position of the animal (McNaughton et al., 1996; Samsonovich and McNaughton, 1997; Conklin and Eliasmith, 2005; Burak and Fiete, 2009).

In insects, the computations pertaining to path integration are believed to occur in the central complex, a brain structure conserved among insect species (Heinze et al., 2013; Pfeiffer and Homberg, 2013; Seelig and Jayaraman, 2015; Weir and Dickinson, 2015; Heinze, 2015; Turner-Evans and Jayaraman, 2016; el Jundi et al., 2018; Franconville et al., 2018). Neurons that encode the animal's heading and speed have been identified in the central complex (Heinze and Homberg, 2007; Homberg et al., 2011; Seelig and Jayaraman, 2015; Green et al., 2017; Stone et al., 2017) and its characteristic columnar structure and regular projection patterns have been hypothesised to provide a plausible substrate for the required path integration computations (Stone et al., 2017).

The existence of the necessary anatomical connectivity for the formation of a bump attractor has been demonstrated in the head direction circuit of insects (Seelig and Jayaraman, 2015; Kim

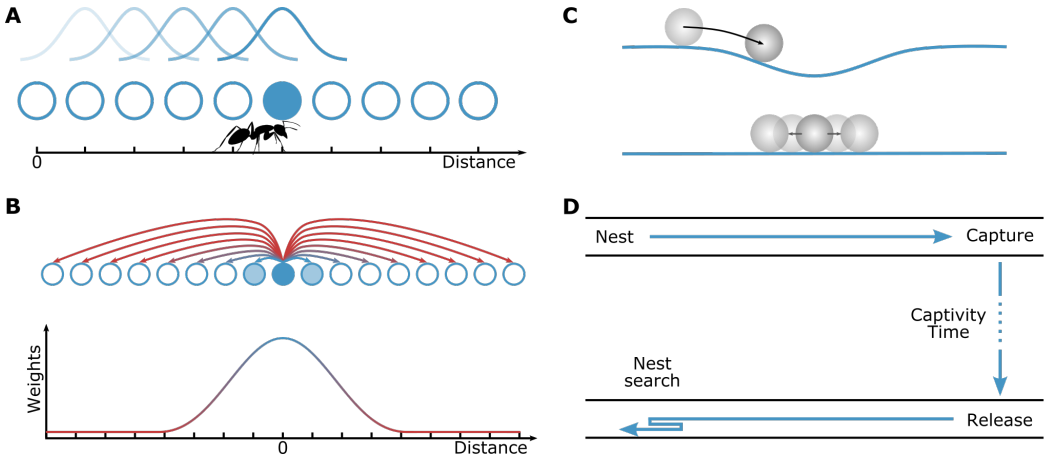

Figure 1: **Bump attractor networks as spatial location memory. (A)** The state of a bump attractor is encoded in the position of the most active neuron in the network. In a bump attractor that integrates an animal's velocity, the location of the activity bump would encode the spatial position of the animal. **(B)** In a bump attractor network, the synaptic connectivity weights pattern results in the formation of one activity bump. The synaptic weights of one exemplar neuron are shown; the same pattern is repeated for all neurons. The synaptic connections (arrows) are colour-coded by their strength, with blue denoting excitatory synapses and red inhibitory synapses. The synaptic strength is a function of the distance from the emanating neuron. **(C)** Inhomogeneities in the biophysical and synaptic properties of the network cause a systematic drift in the bump's location (top of panel), while neuronal noise causes an unbiased stochastic drift of the bump's location (bottom of panel). **(D)** For measuring the homing accuracy of path integration, ants were captured once they reached a feeder, held in captivity for different amounts of time, and then released in a remote unfamiliar location (Ziegler and Wehner, 1997). Upon release, ants that have not been kept in prolonged captivity would typically run towards their expected nest location, not finding it since they are displaced, and perform a focused search for the entrance of their nest. The distance at which ants start searching for their nest is a measure of the memorised home vector distance. The spread of this distance over trials is a measure of the homing accuracy.

et al., 2017; Turner-Evans et al., 2017; Kakaria and de Bivort, 2017; Green et al., 2017; Su et al., 2017; Green and Maimon, 2018; Pisokas et al., 2020; Turner-Evans et al., 2020), but no direct connectomic evidence of bump attractor synaptic structure for encoding translational displacement has been identified in the underlying neural substrate.

Current bump attractor models exhibit limited state stability over time (Brody et al., 2003), while insects can maintain the memory of their home vector for hours (Ziegler and Wehner, 1997). This is an important discrepancy and it is, therefore, imperative to investigate whether bump attractors are an ecologically plausible underlying memory mechanism for path integration. To address this question, we compare the dynamics of bump attractors with those of the path integration memory of the desert ant *Cataglyphis fortis*. If the ant's memory mechanism indeed employs a bump attractor network, its dynamics should be consistent with the ant's behaviour dynamics.

2 Results

2.1 Homing accuracy

The way the homing accuracy of an animal degrades over time could provide crucial information about its spatial memory characteristics. The state of a bump attractor is subject to two phenomena: systematic and stochastic drift. The systematic drift is due to inhomogeneities in network parameters, while the stochastic drift is due to neuronal noise. Both of these would affect the bump's location (Fig 1C). In bump attractors, when no input signal is provided, stochastic neuronal noise

causes the activity bump's location to stochastically drift over time (Compte et al., 2000; Burak and Fiete, 2012). Due to the stochastic drift, the bump increasingly deviates from its original location with a constant rate over time (Fig 2A). Therefore, if the ant's home vector memory were based on a bump attractor network, we would expect a constant increase in the animal's home vector memory error and accordingly a constant deterioration rate in its homing distance accuracy over time.

Two studies have attempted to quantify how the homing accuracy of path integrating ants (*Cataglyphis fortis*) degrades with time (Ziegler and Wehner, 1997; Cheng et al., 2005). The *Cataglyphis fortis* ants are endemic in the salt pans of Tunisia and Algeria, where the skyline is flat, providing no prominent visual cues the animals can use for navigation, so the ants are known to resort to path integration for their navigation (Müller and Wehner, 1988). Therefore, this ant species is a suitable candidate for studying path integration in isolation from other navigational competencies. In the aforementioned studies, the ants were captured once reaching a feeder, away from their nest, and were kept confined in a dark box for different amounts of time before being released at an unfamiliar location. Once released, these ants typically run towards their expected nest location (Fig 1D). The authors measured the distance the ants ran before they started searching for their nest's entrance.

Even though the typical foraging excursion of a *Cataglyphis fortis* ant in its natural habitat lasts no more than one hour, Ziegler and Wehner (1997) found that the ants maintained their home vector memory for several hours, a finding that was confirmed by Cheng et al. (2005) in a similar experiment. We analysed the data reported by these authors and observed that the homing distance error (absolute deviation) increases with a constant rate over time (Fig 2B). This is in accordance with what one would expect from a bump attractor based memory because stochastic drift causes a constant increase in the bump's location deviation and thus does not contradict the bump attractor memory hypothesis.

2.2 Required neuron number

In principle, a bump attractor could reproduce the constant increase of error in homing accuracy, but we see from the behavioural data that the homing accuracy of *Cataglyphis fortis* ants deteriorates over time with a rate of 0.034 m/h (Fig 2B). In bump attractor networks, the bump's location drift rate is inversely proportional to the number of neurons in the network as well as the neuronal time constant (Compte et al., 2000; Burak and Fiete, 2012). Fig 2A, depicts the bump's drift for networks of different sizes. One can notice that the time scales in the abscissa of plots Fig 2A and 2B differ by three orders of magnitude. Thus the question arises, how many neuronal units are required to reproduce the drift rate observed in the ant behavioural experiments?

Since the exact number of neurons depends on the assumptions about the circuit structure and the biophysical properties of the neurons, there is no unique solution. We, therefore, provide as example an indicative solution for a bump attractor implementation with reasonable assumptions about the biophysical neuronal parameters (see Materials and Methods). The result provides an indication of the order of magnitude of required neurons. By plotting the relationship between the network size and the drift rate of the bump's location and extrapolating the fitted curve (Fig 2D, dashed line), we find that the bump attractor network requires a minimum of around 47000 neuronal units for exhibiting a drift rate comparable with that observed in the ants' behaviour (3.4 cm/h). In reality, each neuronal unit in a bump attractor might consist of several neurons, and the circuit would require additional neuronal resources for controlling the bump's shift in response to input signals as well as a population of inhibitory neurons. This means that the actual number of required neurons would be a multiple of 47000.

In insects, this home vector memory has been speculated to lie in the fan-shaped body (also known as the upper central body) of the central complex (Stone et al., 2017; Collett, 2019). The

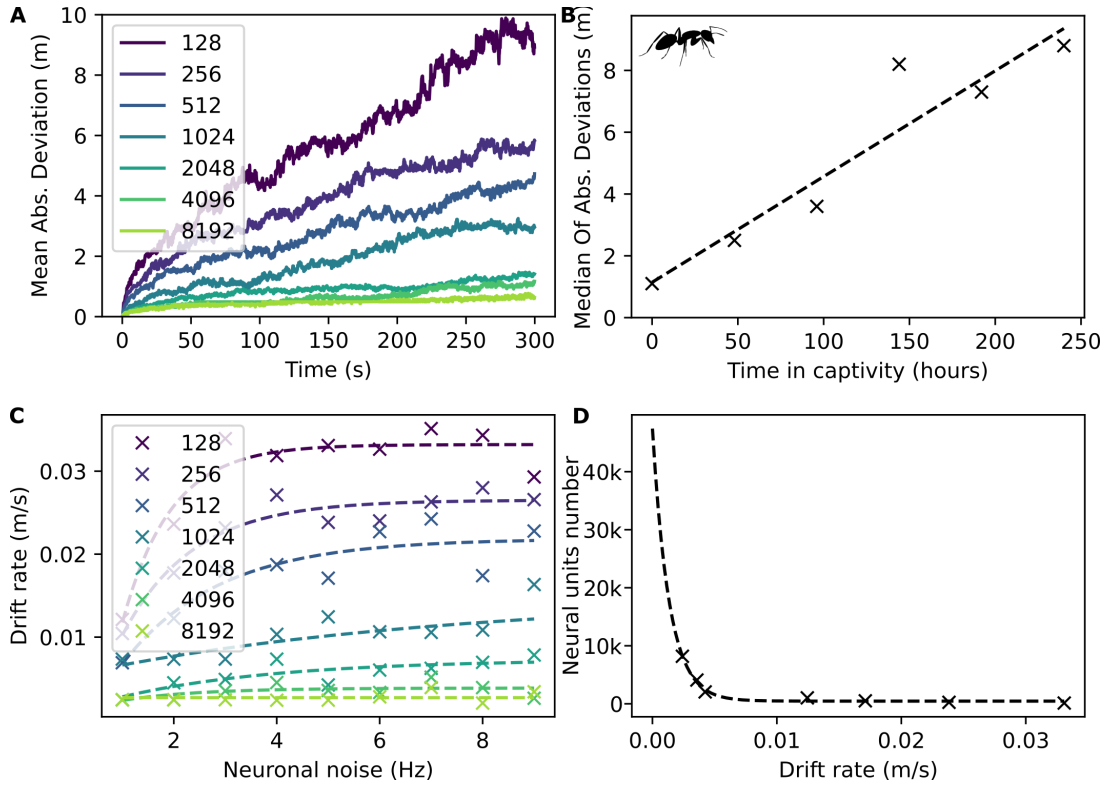

Figure 2: **Path integration error accumulation over time. (A)** Simulation results of the error accumulation in the attractor's activity bump location over time for networks of different sizes. Since homogeneous neuron biophysics and synaptic properties were used, the accumulated error was due to neuronal noise. The error accumulates with a constant rate over time, resulting in a constant increase of the mean absolute deviation of the bump's location from its initial location. An increased number of neuronal units in the bump attractor results in a decreased error accumulation rate. **(B)** The ants' homing distance accuracy degenerates with captivity duration (Data from Ziegler and Wehner (1997)). The line $y = ax + b$ was fitted to the data with parameters $a = 0.034$ and $b = 1.143$ (R^2=0.891) showing that the homing distance error accumulated with a rate of 0.034 m/h. **(C)** Error accumulation rate (drift rate) in the activity bump's location for different attractor network sizes. **(D)** The required number of neurons increases exponentially as the required error accumulation rate decreases. The fitted exponential function (dashed curve) $y = ae^{(-bx)} + c$ has parameters $a = 46969.253$, $b = 746.378$, and $c = 458.977$ (R^2=0.985). Solving by extrapolation for drift rate $0.034m/h$ gives a minimal required network size of 47000 neural units.

exact number of neurons in the ant's brain is not known, but the comparable central complex of *Drosophila melanogaster* is estimated to have no more than 5000 neurons, while the whole brain is estimated to have 200,000 neurons (Raji and Potter, 2021). Current models and neuroanatomical evidence suggest the existence of 8 or 16 independent distance integrators, one for each represented cardinal direction (Stone et al., 2017), and independent distance integrators might exist for path integrating based on optical flow and stride counting self-movement estimation, further increasing the required number of neurons (Collett, 2019). The insect brain does not have enough neurons to accommodate a memory circuit that requires so many neurons to reproduce the drift rate observed in the animals.

2.3 Required neuronal time constant

In the previous section, we assumed that neurons have a typical membrane and synaptic time constant. However, the bump's drift rate also depends on the neuronal time constant and decreases as the time constant increases (Fig 3). If we assume a network of a plausible size, i.e. a few hundreds of neurons (256 neuronal units were used in the simulations), we find that to achieve a

bump attractor with a drift rate of approximately 3.4 cm/h, we would need a neuronal time constant of around $\tau = 60\,000$ s (Fig 3), that is approximately 17 h. This is beyond the time constants range of typical neurons.

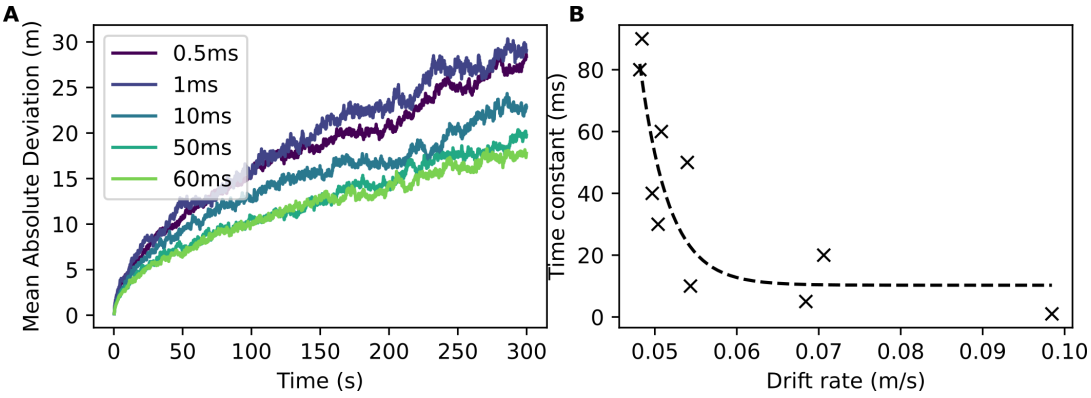

Figure 3: **Effect of time constant on error accumulation. (A)** Simulation results of error accumulation in the bump's location for different neuronal time constants (300 trials for each condition). The error accumulation rate decreases with an increased time constant. A network of 256 neuronal units was used for the simulations. Note the higher error accumulation rate than in Fig 2A due to the use of higher Poisson neuronal noise for the attractor network to sustain a bump at higher neuronal time constants (1400Hz Poisson noise). As the time constant is varied towards lower and higher values its effect is progressively reduced until the model breaks. **(B)** Dependence of error accumulation rate on the neuronal time constant. The fitted exponential function (dashed curve) $y = ae^{(-bx)} + c$ has parameters $a = 62284375$, $b = 283.941$, and $c = 10.277$ (R^2=0.761). Solving by extrapolation for drift rate 3.4 cm/h gives a minimum required neuronal time constant of around 60 000 s (17 h).

2.4 Neurons with a long time constant

One way to increase the time constant of neurons is to replace each neuron with a recurrent neural circuit with positive feedback (Cannon et al., 1983; Seung, 1996). Such recurrent networks may exhibit time constants higher than those of their constituent neurons, however, at the expense of an even larger number of neurons, so they are not a viable solution.

On the other hand, principal neurons in Layer V of the entorhinal cortex (EC) and the lateral nucleus of the lateral amygdala (LA), are able to generate action potentials that are sustained at a constant frequency for prolonged periods of time (Egorov et al., 2002, 2006). These single-neuron oscillators are not dependent on reverberating activity in recurrent circuits, and their spike rate can be gradually increased or decreased with appropriate synaptic input (Egorov et al., 2002; Fransén et al., 2006).

This mechanism, which depends on a non-specific calcium-sensitive cationic current, introduces dynamics operating at a time scale that is many times larger than the time constants of the neuronal membrane and synapses. We, therefore, replaced the neurons in our bump attractor model with a model that included this conductance to investigate whether the prolonged activity phenomenon would result in more stable bump attractor dynamics. Indeed this replacement resulted in a significantly lower bump location drift rate (Fig 4), making such a bump attractor network model seem to be a plausible solution even in the face of the limited number of neurons in an insect's brain. If such neurons exist in insect brains, the required drift rate of 3.4 cm/h could be achievable even with as few as 256 neuronal units. However, so far, graded persistent activity has only been reported in the mammalian brain *in vitro* under very specific non-physiological conditions, and it is unclear whether it is expressed under realistic physiological *in vivo* conditions. It is also unknown if this conductance is expressed in insect neurons.

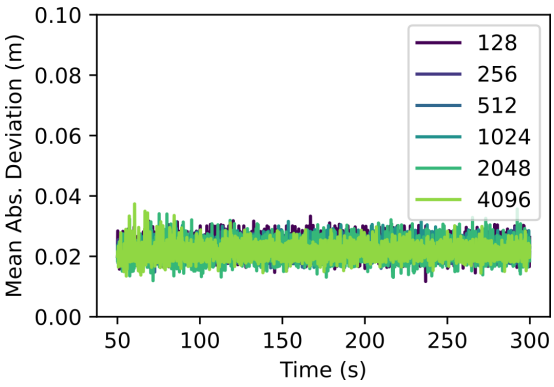

Figure 4: **Bump attractor error accumulation using neurons with a persistent non-specific cation conductance.** Simulation results of error accumulation in the activity bump's location over time for networks of different sizes. Homogeneous neuron biophysics and synaptic properties were used. The median drift rate was less than $0.0001\,\mathrm{m\,s^{-1}}$.

2.5 Homing distance decay regime

There is an additional aspect of the ants' distance memory dynamics that we should consider. In bump attractors, the bump may drift isotropically and equally likely towards higher and lower values (Fig 5A). Therefore, another prediction of the bump attractor hypothesis is that the deterioration of the animal's homing distance accuracy due to memory drift would be equally likely to result in longer or shorter homing distances than the actual distance to the nest. However, the homing distance of the ants systematically and monotonically decreases with time (Fig 5B). This is a fundamental difference between the ant's behaviour and the predicted state loss of bump attractors, rendering the vanilla bump attractor hypothesis an insufficient explanation of the observed behaviour.

It is, however, conceivable that the monotonic decay of the homing distance over time might be due to a systematic bias in the bump attractor network. This systematic bias could be caused by a structural bias in the synaptic weights that would shift the activity bump in one direction over time. We, therefore, tested the effect of introducing bias to the synaptic weights of the bump attractor by replacing the Gaussian synaptic profile (Fig 1B) with a skewed Gaussian synaptic profile (see Materials and Methods Section 4.2). This resulted in systematic biased drift in the bump's location. However, this manipulation produced a constant decay rate (Fig 5C,D) that cannot account for the accelerating decay rate seen in ants (Fig 5B). This suggests that a different process causes homing distance degradation in the animals.

Altering the synaptic bias to produce the accelerating decay regime observed in the animals would require that the biased synaptic profile dynamically changes depending on the initial homing distance. Such dynamic adaptation of the synaptic weights is unrealistic, and would require a substantial neuronal apparatus to manage it, raising the number of required neurons once more.

2.6 Effect of bump drift on agent homing

In animals, memory does not exist in isolation but in the context of a behaving agent. We, therefore, investigated the bump attractor memory model as part of a simulated agent producing behaviour. This allowed us to test whether the agent behaviour would resemble that of the animals. After travelling away from its origin (nest), the agent was held in 'captivity' for different waiting times, and then released for returning to its nest.

Theoretical analysis, neuroanatomical evidence, and modelling work indicate that the insect home vector is stored as a Cartesian vectorial representation with individual memory units storing the coordinate values along each cardinal axis (Fig 6) (Cheung and Vickerstaff, 2010; Vickerstaff and

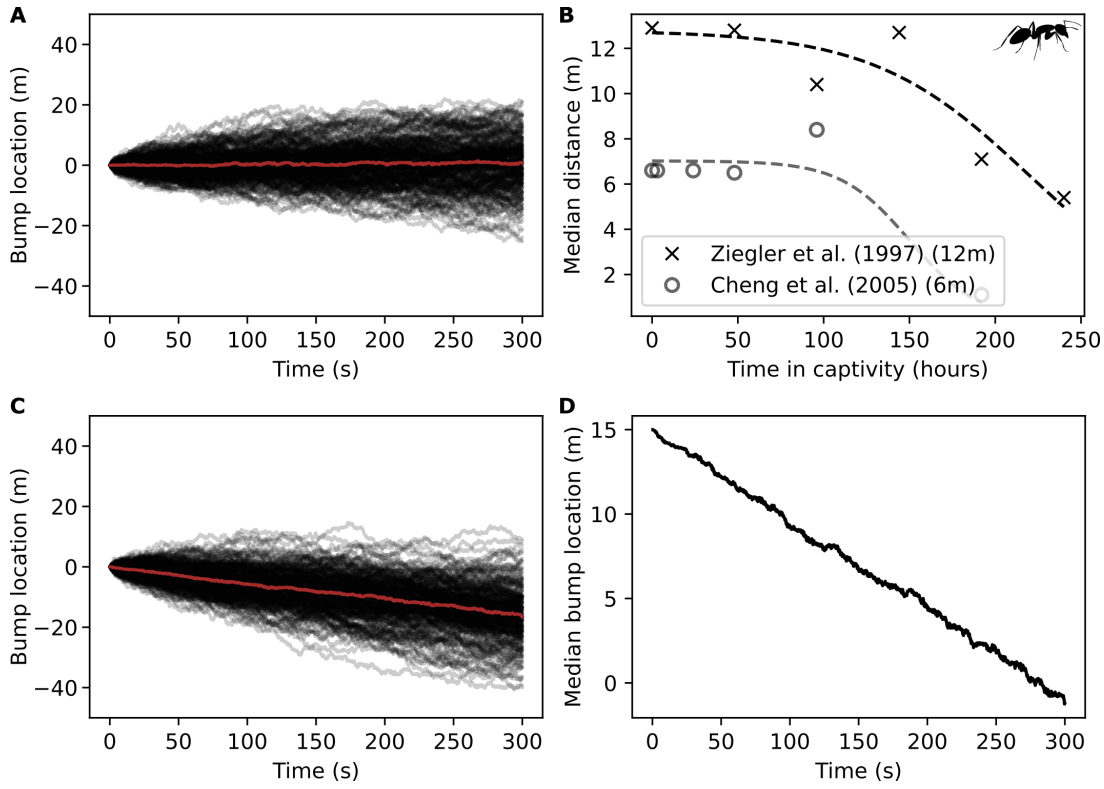

Figure 5: **Loss of state value over time. (A)** Dispersion in the bump attractor's state over time for 200 simulation trials starting from the same initial state of the bump attractor. The initial bump location disperses due to stochastic neuronal noise resulting in increased mean absolute deviation from the original value with a constant rate. During individual trials, the bump is equally likely to move towards higher or lower location values. The median across trials is shown in red. **(B)** The homing distance of ants monotonically decays with captivity time. Data points in black x's are from Ziegler and Wehner (1997), while data points in grey o's are from Cheng et al. (2005). The actual distance between nest and capture point is 12 m in Ziegler and Wehner (1997) and 6 m in Cheng et al. (2005). The inverse logistic function (Boltzmann function) $y = \frac{a}{1+e^{k(x-x_0)}}$ was fitted to the data points with parameter values $a = 12.791$, $x_0 = 219.699$, and $k = 0.022$ (R^2=0.848) for Ziegler and Wehner (1997) and $a = 11.744$, $x_0 = 115.961$, and $k = 0.040$ (R^2=0.866) for Cheng et al. (2005). **(C)** Effect of systematic anisotropy in synaptic weights of the bump attractor. Anisotropy was introduced by changing the synaptic strength pattern from Gaussian to skewed Gaussian with parameter a=-0.0005, resulting in a constant bump drift rate. Data of 200 simulation trials are shown (the median across trials is shown in red). The bump location changes because of the combination of systematic drift due to the structural bias and stochastic drift due to neuronal noise. **(D)** Median bump location of the data shown in **C** with the starting value set to 15 m for comparison with **B**. Unlike the ants, the bump's location drifts with a constant rate.

Cheung, 2010; Wittmann and Schwegler, 1995; Kim and Hallam, 2000; Vickerstaff and Di Paolo, 2005; Haferlach et al., 2007; Stone et al., 2017; Wolff and Rubin, 2018; Hulse and Jayaraman, 2020; Pisokas et al., 2021). Modelling has shown that the columnar organisation of the central complex provides a neural basis for potentially encoding and storing the coordinate values along eight columns of neurons, with each column corresponding to a cardinal axis (Haferlach et al., 2007; Stone et al., 2017). In this model, the eight memory values form a sinusoidal pattern with its amplitude encoding the distance the agent has travelled away from its origin and the location of the minimal memory value (column) corresponding to the direction the agent has mostly travelled away from its origin (Fig 6C) (Haferlach et al., 2007; Stone et al., 2017). When a homing agent returns to its origin, the sinusoid's amplitude approaches zero and does not provide the agent with a direction to move towards. As a result, a homing agent would move in a random pattern around the expected nest location, resembling the search pattern observed in ants (Stone et al., 2017).

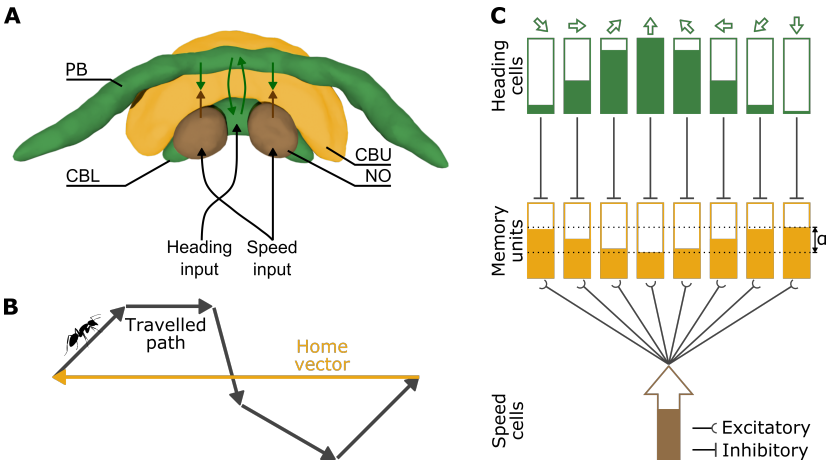

Figure 6: **A Cartesian home vector encoding model of insect path integration. (A)** The anatomy of the central complex and the main neuronal signal pathways involved in path integration. The brain structures — protocerebral bridge (PB), upper central body (CBU, also fan-shaped body), lower central body (CBL, also ellipsoid body), and noduli (NO) — are colour coded to match the conceptual drawing in **C**. The compartment and arrow colours indicate the type of identified signals (heading and speed) and their convergence in the CBU, where the path integration memory is hypothesised to reside (Stone et al., 2017). Image adapted from the insectbraindb.org. **(B)** Illustration of example outbound path and corresponding accumulated home vector. **(C)** Conceptual depiction of the path integration model with each of the eight columns encoding one of the cardinal directions in a Cartesian coordinate system (Stone et al., 2017). Rectangular boxes represent neuronal ensembles and shaded portions the activity level or stored value. The inputs are the current insect heading (population coding with eight cardinal directions around the animal, i.e. EPG neurons (Wolff and Rubin, 2018)) and the current insect speed (encoded as the spike rate of TN neurons (Stone et al., 2017)). Both the heading and speed neurons drive the eight speed integrating 'memory units'. The inhibitory heading signals mask the speed signal, so the lower the heading neuron activity, the more the speed signal is integrated by the corresponding memory unit. The memory unit values form a sinusoidal pattern encoding the distance from the origin in its amplitude (α) and the direction to the origin in the horizontal location of the minimum.

In our model, each memory unit consists of a bump attractor encoding the agent's displacement in the corresponding cardinal direction. We assumed that the bump attractors have neurons with a large enough time constant resulting in the homing accuracy decay rate observed in ants (3.4 cm/h). During the waiting time the bump attractors would accumulate error. As expected, the agent's homing distance and direction accuracy degraded with the waiting time before release (Fig 7). We also observed that the decay of the directional accuracy was similar to the decay of the distance accuracy (compare 7C and 7D). This is in contrast to the ants' behaviour, where the distance accuracy decays faster than the directional accuracy (Ziegler and Wehner, 1997). Clearly, the animal's memory follows dissipation dynamics that do not match the diffusion dynamics of attractor networks. Furthermore, the median homing distance of the agent slightly increased with the waiting time (Fig 7D, non statistically significant change), while in the ants systematically decreased with an accelerating rate (Fig 5B). These findings show that even in the context of a behaving agent, the bump attractor dynamics do not produce behaviour resembling that of the animals.

3 Discussion

We investigated the plausibility of the bump attractor model as a potential mechanism underlying path integration memory in insects. To this end, we compared the temporal dynamics of the path integration memory of *Cataglyphis fortis* ants with those of bump attractors encoding the agent's displacement. While the behaviour of bump attractors depend on the choice of modelling

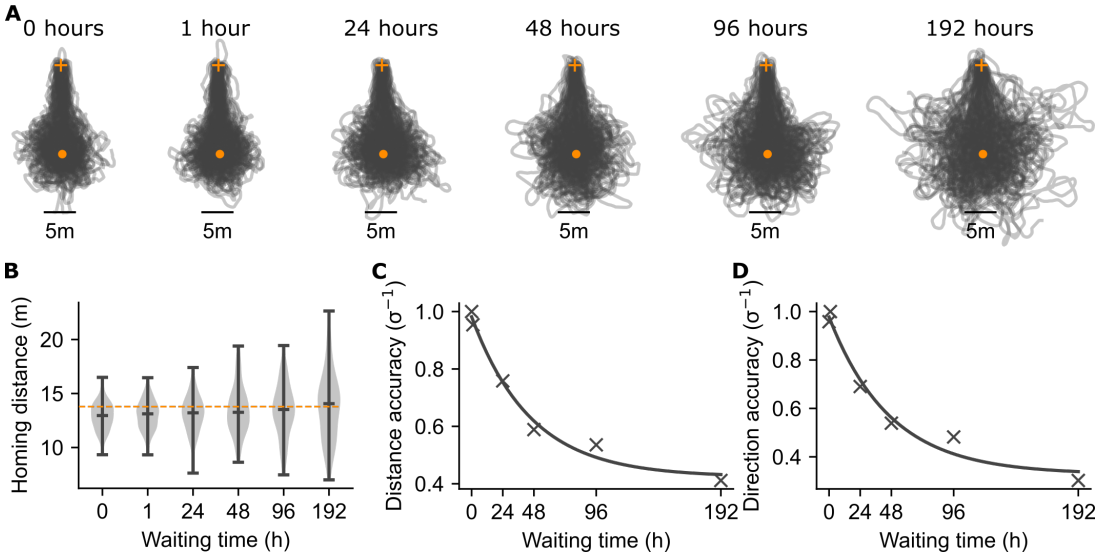

Figure 7: **Agent homing accuracy degradation over time. (A)** Paths of an agent kept stationary (waiting) for different amounts of time before being released for homing. The release location is indicated with an orange cross and the nest location with an orange disc. During the waiting time the bump attractor's state stochastically drifts accumulating error. Then the agent is released to return to its origin as indicated by its home vector memory (encoded in the state of the bump attractors). Once the agent reaches the location indicated by its memory, it searches following a random looping trajectory resulting in the blob of overlapping paths centered at the expected home location (orange disc). **(B)** The distribution of the homing distances (distance between the release point and the focus of search) as a function of the waiting time. **(C)** The median homing distance accuracy as a function of the waiting time. The fitted exponential function (dashed curve) $y = ae^{(-bx)} + c$ has parameters $a = 0.558$, $b = 0.022$, and $c = 0.424$. **(D)** The mean homing direction accuracy as a function of the waiting time. Fitted with an exponential function with parameters $a = 0.649$, $b = 0.021$, and $c = 0.328$.

assumptions and parameters, we found that certain properties are robust features of this model class, which we compared to experimental data. We tested the bump attractor hypothesis with respect to the temporal degradation dynamics of homing accuracy, the number of required neurons, and the required neuronal time constants.

The bump attractor hypothesis predicts that the accuracy of the ants' homing distance degrades at a constant rate during the period of time intervening before release. This is indeed the case in *Cataglyphis fortis* ants. The bump attractor hypothesis also predicts that the bump attractor network must consist of a considerable number of neurons or of neurons with adequately high time constants to be stable enough at the ecologically relevant time scale. However, the corporeal reality of the insect brain renders this last prediction inadmissible since it neither contains enough neurons nor are they known to have the high time constants required. But even in the case that these conditions are satisfied by a yet unobserved physiological property substantially increasing the neuronal time constant, we showed that the state value drift dynamics predicted by the bump attractor hypothesis do not match the observed dynamics of the animal's homing distance. Any reasonable attempt to coax the bump attractor into reproducing the animal homing distance dynamics has failed.

In the present work, we assumed that the homing distance degradation in ants is due to a degradation in the animal's path integration memory. It is not inconceivable that other factors might be involved in the observed behaviour, such as the motivational state of the animals. However, there was no evidence of such an effect in the experiments since the animals continued searching for their nest, indicating that they were motivated to return to it.

A further consideration is that the biophysical parameters used in our models are based on measurements performed on neurons *in vitro*, typically at room temperatures. The desert ants,

Table 1: Ant and bump attractor dynamics comparison.

Parameter	Ants	Bump Attractor
Distance decay type	Monotonic	Random walk
Distance degradation rate	Constant	Constant
Number of neurons	Limited	More than available
Resettable	Yes	Yes

Cataglyphis fortis, are active at much higher temperatures which unavoidably affect the biophysical properties of their neurons. At higher temperatures, the membrane ion-channels become faster (Frankenhaeuser and Moore, 1963; Tang et al., 2010), their conductance increases (Volgushev et al., 2000), and synaptic transmission is faster (Postlethwaite et al., 2007). The structural properties of the membrane are also affected, resulting in decreased capacitance and time constants (Volgushev et al., 2000), while the neuronal channel noise level decreases (Faisal et al., 2005, 2008). The precise effect of the higher temperature on the neurons is complex and further investigation is needed. However, the magnitude and polarity of the effects of temperature seem unlikely to result in a significant coordinated improvement of the bump attractor's stability.

Despite our attempts to address every one of the model's limitations, the bump attractor hypothesis failed to withstand all our tests. The model is limited both in the duration of state maintenance and the dynamics of state degradation. Our work falsifies the bump attractor memory hypothesis and rekindles the quest for the memory substrate of path integration.

4 Materials and Methods

4.1 Data extraction and processing

The ant behaviour data were extracted from Ziegler and Wehner (1997) and Cheng et al. (2005). The extracted data points as well as the data produced from simulations in this paper were fitted using the curve_fit function of SciPy's optimize Python package with curve parametrisation as described in Figs 2, 3, 5, and 7.

4.2 Bump attractor network model

The bump attractor network model implementation used in our experiments was derived from the code of Gerstner et al. (2014). Our source code is available at `https://github.com/johnpi/Pisokas_Hennig_2022_Attractor_Based_Memory`. To avoid the effect of boundary conditions at the edges of a line attractor, we used a ring attractor network topology and we made sure our experiments were confined to activity bump shifts less than $\pm 180°$. In this way, for the purposes of our experiments the topology of the circuit was indistinguishable from an actual line attractor.

The bump attractor network model used in the experiments had uniform global inhibition and structured lateral excitatory synapses with efficacies that followed a Gaussian profile. The skewed Gaussian formulation described below was used for determining synaptic efficacies to allow us to choose between Gaussian and skewed Gaussian profiles. The synaptic efficacies $w(x_i, x_j)$ were therefore described by the following formulation. Let $\phi(x)$ denote the Gaussian probability density function

$$\phi(x) = \frac{1}{\sigma\sqrt{2\pi}} e^{-\frac{1}{2}(\frac{x}{\sigma})^2}$$

where $\sigma^2 = 20$ is the variance (width) of the Gaussian profile. Let $\Phi(x)$ denote the cumulative distribution function of the Gaussian

$$\Phi(x) = \int_{-\infty}^{x} \phi(y)\, dy = \frac{1}{2}\left[1 + \text{erf}\left(\frac{x}{\sigma\sqrt{2}}\right)\right]$$

where $erf(\cdot)$ is the error function. Then the probability density function of the skewed Gaussian and thus the synaptic weights are given by

$$w(x_i, x_j) = 2\phi(x_i - x_j)\Phi(\alpha(x_i - x_j))$$

where α is the skewness factor, with $\alpha = 0$ resulting in the Gaussian probability density function. In the case of simulations with systematically biased bump drift we used $\alpha = -0.0005$. x_i and x_j are the positions of the presynaptic and postsynaptic neurons, and $w(x_i, x_j) \in [-1, 1]$ is the synaptic connection weight from neuron x_i to neuron x_j. The values of x_i and x_j are periodic taking values in the range $[0, N-1]$, where N is the number of excitatory neuronal units in the circuit and the difference $x_i - x_j$ is calculated as a modulo N subtraction, as in Brody et al. (2003). The values of $w(x_i, x_j)$ determined the synaptic efficacy profile of the excitatory synapses while the inhibitory synapses had uniform efficacy.

4.3 Neuron model

We used two neuronal models in our experiments. The first one, the base model, utilised spiking neurons with AMPA, NMDA and $GABA_A$ receptor channels. The inclusion of NMDA receptors endows the network with regular activity, since a network with only AMPA and $GABA_A$ receptors produces synchronous spiking activity (Compte et al., 2000).

The second neuron model, utilised the neurotransmitter receptors of the first model and in addition cholinergic muscarinic receptors (mACh) that metabotropically opened clusters of cooperative non-specific cation channels that provided the graded persistent spiking observed in the entorhinal cortex layer V neurons (Egorov et al., 2002, 2006).

The intrinsic neuronal properties for the excitatory neurons of the base model were set to a membrane capacitance $C_m = 0.5nF$, leak conductance $g_L = 25nS$, reversal potential $E_L = -70mV$, threshold potential $V_{th} = -50mV$, reset potential $V_{res} = -60mV$, and absolute refractory period $\tau_{ref} = 2ms$. For the inhibitory neurons of the base model the corresponding values were $C_m = 0.2nF$, $g_L = 20nS$, $E_L = -70mV$, $V_{th} = -50mV$, $V_{res} = -60mV$, and $\tau_{ref} = 1ms$.

The intrinsic neuronal properties for the excitatory neurons with the non-specific cation conductance were set to a membrane capacitance $C_m = 0.2nF$, leak conductance $g_L = 0.2nS$, reversal potential $E_L = -63mV$, threshold potential $V_{th} = 10mV$, reset potential $V_{res} = -60mV$, and absolute refractory period $\tau_{ref} = 3ms$. For the inhibitory neurons with the non-specific cation conductance the corresponding values were $C_m = 0.2nF$, $g_L = 0.2nS$, $E_L = -63mV$, $V_{th} = 10mV$, $V_{res} = -60mV$, and $\tau_{ref} = 2ms$.

For modifying the membrane time constant of the neurons the membrane capacitance was adjusted accordingly using the equation

$$C_m = \tau_m * g_L$$

where τ_m is the desired time constant. The external input that sets the initial bump location consists of synaptic connections formed with the excitatory neurons that are mediated by AMPA receptors. The maximum conductance of AMPA receptors channels for the excitatory cells was $G_{ext,E} = 3.1nS$ and for the inhibitory cells $G_{ext,I} = 2.38nS$.

Postsynaptic currents were modeled as

$$I_{post} = sg_{syn}(V_m - E_{syn})$$

where s is the gating variable, g_{syn} the synaptic conductance, V_m the membrane potential, and E_{syn} the synaptic reversal potential (set to 0mV for AMPA, NMDA, and mACh receptor channels and to -70mV for $GABA_A$ ones). The gating variables were modeled as in Compte et al. (2000). The decay time constants of the gating variables were set to 2ms for AMPA, 10ms for $GABA_A$, 65ms for NMDA, and 5ms for mACh receptor channels.

The non-specific cation channels were modelled as clusters of cooperatively opening channels (Pfeiffer et al., 2020). The cluster opening kinetics were governed by

$$\frac{dO_{coop}}{dt} = \frac{\alpha_o}{\tau_{coop}} s_{mACh} G_{EE} - \frac{\beta_o}{\tau_{coop}} s_{GABA} G_{IE}$$

where α_o and β_o are the opening and closing rate factors, respectively. τ_{coop} is the average cluster transition time constant. s_{mACh} and s_{GABA} are the channel gating variables. G_{EE} and G_{IE} are synaptic conductances described in Table 2. The number of open clusters was clipped to the range [0, 100]. The total cluster current was

$$I_{cluster} = G_{coop} O_{coop} (V_m - E_{coop})$$

where $G_{coop} = 0.4nS$. The synaptic conductance between neurons i and j was modeled as

$$g_{syn,ij} = w(x_i, x_j) G_{syn}$$

The synaptic conductances G_{syn} mediated by the AMPA, NMDA, $GABA_A$, and mACh (cholinergic muscarinic) receptor channels were determined by following the procedure outlined in Brody et al. (2003) to obtain the formation of a stable activity bump. Subsequently, starting with the hand tuned values, the dual_annealing optimiser from SciPy' optimize Python package was utilised to optimise the synaptic conductances G_{syn} using the objective function

$$\begin{aligned}
\underset{\mathbf{G}}{\text{argmin}} \quad & \epsilon_{H1}(\mathbf{G}) + \epsilon_{H2}(\mathbf{G}) + 5(\epsilon_{W1}(\mathbf{G}) + \epsilon_{W2}(\mathbf{G})) + \epsilon_{A1}(\mathbf{G}) + \epsilon_{A2}(\mathbf{G}) + 2\epsilon_S(\mathbf{G}) + W_{diff}(\mathbf{G}) \\
\text{s. t.} \quad & \epsilon_{H1}(\mathbf{G}) = \frac{|H_d(t_1) - H_a(\mathbf{G}, t_1)|}{360^\circ} \\
& \epsilon_{H2}(\mathbf{G}) = \frac{|H_d(t_2) - H_a(\mathbf{G}, t_2)|}{360^\circ} \\
& \epsilon_{W1}(\mathbf{G}) = \frac{|55^\circ - W_a(\mathbf{G}, t_1)|}{360^\circ} \\
& \epsilon_{W2}(\mathbf{G}) = \frac{|55^\circ - W_a(\mathbf{G}, t_2)|}{360^\circ} \\
& A_1(\mathbf{G}) = \frac{1}{1 + (A_{max}(\mathbf{G}, t_1, \Delta t) - A_{min}(\mathbf{G}, t_1, \Delta t))} \\
& A_2(\mathbf{G}) = \frac{1}{1 + (A_{max}(\mathbf{G}, t_2, \Delta t) - A_{min}(\mathbf{G}, t_2, \Delta t))} \\
& W_{diff}(\mathbf{G}) = \frac{|W_a(\mathbf{G}, t_1) - W_a(\mathbf{G}, t_2)|}{360^\circ} \\
& 0 \leq G_{II} \leq 0.01 \\
& 0 \leq G_{IE} \leq 10 \\
& 0 \leq G_{EE} \leq 10 \\
& 0 \leq G_{EI} \leq 10
\end{aligned} \tag{1}$$

Where ϵ_{H1}, ϵ_{H2}, ϵ_{W1}, and ϵ_{W2} are the error factors measured as deviations from the desired values. $H_d(t)$ is the desired activity 'bump' heading at time t, while $H_a(\mathbf{G}, t)$ is the actual measured activity 'bump' heading at time t given a model with channel efficacies $\mathbf{G}$. $W_a(\mathbf{G}, t)$ is the actual

Table 2: Ant and bump attractor dynamics comparison.

Conductance variable	Corresponding synapse and receptors
G_{II}	From inhibitory to inhibitory neurons ($GABA_A$)
G_{IE}	From inhibitory to excitatory neurons ($GABA_A$)
G_{EE}	From excitatory to excitatory neurons (NMDA and mACh)
G_{EI}	From excitatory to inhibitory neurons (NMDA and AMPA)

measured width of the activity 'bump' at time t (measured as the full width at half maximum). $A_{max}(\mathbf{G}, t, \Delta t)$ and $A_{min}(\mathbf{G}, t, \Delta t)$ are the maximum and minimum neuron spike rates across all excitatory neurons in the attractor network with channel conductances $\mathbf{G}$, measured for a duration Δt starting at time t. t_1 and t_2 are sampling times located near the beginning and the end of the simulation, respectively. $\mathbf{G}$ is the vector $[G_{II}, G_{IE}, G_{EE}, G_{EI}]$. G_{II}, G_{IE}, G_{EE}, and G_{EI} are the synaptic conductances as described in Table 2. These were optimised separately for the basic model and the model that included the non-specific cation conductances. The synaptic conductances that resulted from multiple runs were manually tested to verify the results.

4.4 Neuronal noise

All neurons receive excitatory input modeled as uncorrelated Poisson spike trains with average spike rate as specified in the appropriate sections of the text. The neuronal noise used in Figures 2A, 2C, 2D, 4, 5A, 5C, and 5D was modeled as Poisson noise with an average spike rate 5 Hz. This noise level was chosen because the attractor's state drift rate reaches a plateau beyond Poisson neuronal noise with an average spike rate of 4Hz (Fig 2C). In Fig 3, the Poisson neuronal noise was set to an average spike rate 1400 Hz to allow networks with higher neuronal time constants to sustain a bump of activity.

4.5 Agent simulations

The agent simulations were based on the anatomically constrained model of Stone et al. (2017). The source code of the original work was modified and extended as described below and it is available at `https://github.com/johnpi/Pisokas_Hennig_2022_Attractor_Based_Memory`. The neurons were modeled as rate-based perceptrons with a sigmoid activation function. Independent Gaussian noise with $\mu = 0$ and $\sigma^2 = 0.01$ was added to the activation of each neuron and the resulting values were clipped to the range $[0, 1]$.

To reproduce agent paths resembling those of ants we added motor noise that is parametric to the home vector length, as in Pisokas et al. (2021). This motor noise was modelled as a Gaussian noise factor applied to the steering commands of the agent

$$steering = steering\_command \cdot \epsilon \tag{2}$$

where $steering\_command$ is the steering command generated by the path integration model in homing mode, $steering$ is the actual agent steering, and $\epsilon \sim \mathcal{N}(\mu, \sigma^2)$ is a random variable sampled from the Gaussian distribution with $\mu = 1$ and σ set to the motor noise level. The motor noise level was modelled as a decaying exponential function of the memory amplitude, as in Pisokas et al. (2021). The memory amplitude a_m was defined as the difference between the maximum and minimum value along the sinusoidal pattern of memory unit values (Pisokas et al., 2021).

$$Motor\ noise = \frac{y_{max}}{e^{s_m \cdot a_m}} \tag{3}$$

where y_{max} is the maximum motor noise level (corresponding to zero vector ant paths), and s_m is the slope of the exponential function.

The translational velocity of the simulated agents during homing was iteratively updated using the formula

$$v(t) = \begin{cases} v(t-1) + a\Delta t - \mu_f v(t-1), & \text{if } |steering| \leq 20^o \\ v(t) = 0, & \text{if } |steering| > 20^o \end{cases} \tag{4}$$

where $v(t)$ is the agent's velocity at time step t, $a = 0.08\,\mathrm{m/s^2}$ is an acceleration constant, Δt is the simulated time step duration, and $\mu_f = 0.15$ is a friction constant. The velocity was reset to $0\,\mathrm{m/s}$ whenever the agent performed a turn larger than $20°$ simulating a stop on turning as observed in ants (Pisokas et al., 2021).

We performed a grid search following the procedure outlined in Pisokas et al. (2021) to find the combination of maximum motor noise level ($y_{max} = 7$) and slope ($s_m = 9$) of the decaying exponential that produces simulated paths that resemble the paths of both zero vector ants (zero memory amplitude) and full vector ants.

The inputs to the path integration model were the allocentric orientation of the agent and the speed of the agent's motion (Figure 6, see also Stone et al. (2017)). Visual landmark cues were not used in either the outbound or the homing part of the simulations; thus, path integration was the sole navigation mechanism utilised. The simulations had two stages, an outbound trip and a homing trip. For generating the outbound trip, the agent begun from a designated nest location and moved following a path generated by a filtered (smoothed) noise process, as previously described by Stone et al. (2017), until it reached a designated food location. Outbound agent simulations that did not result in the agent reaching the designated food location after 1500 simulation steps were disregarded. During the outbound trip, a home vector was accumulated that was encoded as the states of the eight memory units. Subsequently, an intervening waiting period was simulated during which stochastic memory state drift continued to occur, and then the simulation proceeded with the agent release in homing mode. The simulated homing paths were cut at 1500 steps from release allowing a sufficiently long observation period of the search behaviour to estimate the centre of search.

4.6 Agent memory model

For computational efficiency, the bump attractor memory dynamics were introduced in the agent simulations as variables with Brownian noise that replicated the stochastic drift exhibited by the bump attractors. The states of the memory units were updated by

$$mem(t) = mem(t) + b \tag{5}$$

where

$$b \sim \mathcal{N}(\mu, \sigma^2) \tag{6}$$

There were eight such variables one for each cardinal direction (Fig 6C). We set $\mu = 0$ and σ to appropriate values corresponding to the effect of stochastic bump location drift for the different waiting periods. We experimentally determined that $\sigma = 0.0055$ produces the nearest approximation to the $3.4\,\mathrm{cm/h}$ drift rate observed in the ant behaviour. For different waiting periods the required σ value is given by $\sigma = \sqrt{t_w}0.0055$, where t_w is the waiting period in seconds.

5 Acknowledgements

We would like to thank Barbara Webb for early discussion of the ideas developed in this paper and her comments on the draft. We would also like to thank Eve Marder and Stanley Heinze for early discussion of this work. Part of this work was funded by the Principal's Career Development Scholarship, University of Edinburgh.

References

Christian Boucheny, Nicolas Brunel, and Angelo Arleo. A continuous attractor network model without recurrent excitation: Maintenance and integration in the head direction cell system. *Journal of Computational Neuroscience*, 18(2):205–227, March 2005. ISSN 0929-5313. doi: 10.1007/s10827-005-6559-y.

Carlos D Brody, Ranulfo Romo, and Adam Kepecs. Basic mechanisms for graded persistent activity: Discrete attractors, continuous attractors, and dynamic representations, 2003. ISSN 0959-4388. URL `http://www.sciencedirect.com/science/article/pii/S0959438803000503`.

Yoram Burak and Ila R. Fiete. Accurate Path Integration in Continuous Attractor Network Models of Grid Cells. *PLoS Computational Biology*, 5(2):e1000291, February 2009. ISSN 1553-7358. doi: 10.1371/journal.pcbi.1000291.

Yoram Burak and Ila R. Fiete. Fundamental limits on persistent activity in networks of noisy neurons. *Proceedings of the National Academy of Sciences*, 109(43):17645–17650, October 2012. ISSN 0027-8424. doi: 10.1073/PNAS.1117386109. URL `https://www.pnas.org/content/109/43/17645`.

Stephen C. Cannon, David A. Robinson, and Shihab Shamma. A proposed neural network for the integrator of the oculomotor system. *Biological Cybernetics*, 49(2):127–136, 1983. ISSN 0340-1200. doi: 10.1007/bf00320393.

Ken Cheng, Ajay Narendra, and Rüdiger Wehner. Behavioral ecology of odometric memories in desert ants: Acquisition, retention, and integration. *Behavioral Ecology*, 17(2):227–235, December 2005. ISSN 1045-2249. doi: 10.1093/beheco/arj017.

Allen Cheung and Robert Vickerstaff. Finding the way with a noisy brain. *PLoS Computational Biology*, 6(11):e1000992, 2010. ISSN 1553-734X. doi: 10.1371/journal.pcbi.1000992.

T.S. Collett. Path integration: how details of the honeybee waggle dance and the foraging strategies of desert ants might help in understanding its mechanisms. *Journal of Experimental Biology*, 222, May 2019. ISSN 1477-9145. doi: 10.1242/jeb.205187. URL `http://www.ncbi.nlm.nih.gov/pubmed/31152122`.

A. Compte, Nicolas Brunel, Patricia S. Goldman-Rakic, and Xiao-Jing Wang. Synaptic Mechanisms and Network Dynamics Underlying Spatial Working Memory in a Cortical Network Model. *Cerebral Cortex*, 10(9):910–923, September 2000. ISSN 1460-2199. doi: 10.1093/cercor/10.9.910.

John Conklin and Chris Eliasmith. A controlled attractor network model of path integration in the rat. *Journal of Computational Neuroscience*, 18(2):183–203, March 2005. ISSN 0929-5313. doi: 10.1007/s10827-005-6558-z.

Charles Darwin. Origin of Certain Instincts. *Nature*, 7:417–418, 1873. URL `https://www.nature.com/articles/007417a0`.

Alexei V. Egorov, Bassam N. Hamam, Erik Fransén, Michael E. Hasselmo, and Angel A. Alonso. Graded persistent activity in entorhinal cortex neurons. *Nature*, 420(6912):173–8, November 2002. ISSN 0028-0836. doi: 10.1038/nature01171. URL `http://www.nature.com/doifinder/10.1038/nature01171http://www.ncbi.nlm.nih.gov/pubmed/12432392`.

Alexei V. Egorov, Klaus Unsicker, and Oliver Von Bohlen Und Halbach. Muscarinic control of graded persistent activity in lateral amygdala neurons. *European Journal of Neuroscience*, 24(11): 3183–3194, 2006. ISSN 0953-816X. doi: 10.1111/j.1460-9568.2006.05200.x.

Basil el Jundi, Eric J. Warrant, Keram Pfeiffer, and Marie Dacke. Neuroarchitecture of the dung beetle central complex. *Journal of Comparative Neurology*, 526(16):2612–2630, August 2018. ISSN 1096-9861. doi: 10.1002/cne.24520.

A. Aldo Faisal, John A. White, and Simon B. Laughlin. Ion-Channel Noise Places Limits on the Miniaturization of the Brain's Wiring. *Current Biology*, 15(12):1143–1149, 2005. ISSN 0960-9822. doi: 10.1016/j.cub.2005.05.056.

A. Aldo Faisal, Luc P. J. Selen, and Daniel M. Wolpert. Noise in the nervous system. *Nature Reviews Neuroscience*, 9(4):292–303, 2008. ISSN 1471-003X. doi: 10.1038/nrn2258.

Romain Franconville, Celia Beron, and Vivek Jayaraman. Building a functional connectome of the Drosophila central complex. *eLife*, 7, August 2018. ISSN 2050-084X. doi: 10.7554/elife.37017. URL `https://elifesciences.org/articles/37017`.

B. Frankenhaeuser and L. E. Moore. The effect of temperature on the sodium and potassium permeability changes in myelinated nerve fibres of Xenopus laevis. *The Journal of Physiology*, 169 (2):431–437, 1963. ISSN 1469-7793. doi: 10.1113/jphysiol.1963.sp007269.

Erik Fransén, Babak Tahvildari, Alexei V. Egorov, Michael E. Hasselmo, and Angel A. Alonso. Mechanism of Graded Persistent Cellular Activity of Entorhinal Cortex Layer V Neurons. *Neuron*, 49(5):735–746, March 2006. URL `https://www.sciencedirect.com/science/article/pii/S0896627306000924http://www.sciencedirect.com/science/article/pii/S0896627306000924`.

Wulfram Gerstner, Werner M Kistler, Richard Naud, and Liam Paninski. *Neuronal dynamics: From single neurons to networks and models of cognition*. Cambridge University Press, 2014. ISBN 1107060834.

Dennis Goldschmidt, Sakyasingha Dasgupta, Florentin Wörgötter, and Poramate Manoonpong. A neural path integration mechanism for adaptive vector navigation in autonomous agents. In *2015 International Joint Conference on Neural Networks (IJCNN)*, pages 1–8, 2015. ISBN 9781479919604. doi: 10.1109/IJCNN.2015.7280400.

Dennis Goldschmidt, Poramate Manoonpong, and Sakyasingha Dasgupta. A Neurocomputational Model of Goal-Directed Navigation in Insect-Inspired Artificial Agents. *Frontiers in Neurorobotics*, 11:1–17, April 2017. ISSN 1662-5218. doi: 10.3389/fnbot.2017.00020.

Jeremy P. Goodridge and David S. Touretzky. Modeling Attractor Deformation in the Rodent Head-Direction System. *Journal of Neurophysiology*, 83(6):3402–3410, June 2000. ISSN 0022-3077. doi: 10.1152/jn.2000.83.6.3402.

Jonathan Green and Gaby Maimon. Building a heading signal from anatomically defined neuron types in the Drosophila central complex. *Current Opinion in Neurobiology*, 52:156–164, October 2018. ISSN 1873-6882. doi: 10.1016/j.conb.2018.06.010. URL `https://www.sciencedirect.com/science/article/pii/S0959438818300072`.

Jonathan Green, Atsuko Adachi, Kunal K. Shah, Jonathan D. Hirokawa, Pablo S. Magani, and Gaby Maimon. A neural circuit architecture for angular integration in Drosophila. *Nature*, 546 (7656):101–106, May 2017. ISSN 1476-4687. doi: 10.1038/nature22343.

Thomas Haferlach, Jan Wessnitzer, Michael Mangan, and Barbara Webb. Evolving a neural model of insect path integration. *Adaptive Behavior*, 15(3):273–287, September 2007. ISSN 1059-7123. doi: 10.1177/1059712307082080.

Stanley Heinze. Neuroethology: Unweaving the senses of direction, November 2015. ISSN 0960-9822. URL `http://linkinghub.elsevier.com/retrieve/pii/S0960982215010829`.

Stanley Heinze and Uwe Homberg. Maplike Representation of Celestial E-Vector Orientations in the Brain of an Insect. *Science*, 315(5814):995–997, February 2007. doi: 10.1126/science.1135531. URL `http://science.sciencemag.org/content/315/5814/995.fullhttp://science.sciencemag.org.ezproxy.is.ed.ac.uk/content/315/5814/995.full`.

Stanley Heinze, Jeremy Florman, Surainder Asokaraj, Basil El Jundi, and Steven M. Reppert. Anatomical basis of sun compass navigation II: The neuronal composition of the central complex of the monarch butterfly. *Journal of Comparative Neurology*, 521(2):267–298, February 2013. ISSN 0021-9967. doi: 10.1002/cne.23214.

Stanley Heinze, Ajay Narendra, and Allen Cheung. Principles of Insect Path Integration. *Current Biology*, 28(17):R1043—R1058, 2018. ISSN 0960-9822. doi: 10.1016/j.cub.2018.04.058. URL `https://www.sciencedirect.com/science/article/pii/S096098221830530Xhttps://linkinghub.elsevier.com/retrieve/pii/S096098221830530X`.

Uwe Homberg, Stanley Heinze, Keram Pfeiffer, Michiyo Kinoshita, and Basil El Jundi. Central neural coding of sky polarization in insects. *Philosophical Transactions of the Royal Society B: Biological Sciences*, 366(1565):680–687, 2011. ISSN 1471-2970. doi: 10.1098/rstb.2010.0199. URL `http://rstb.royalsocietypublishing.org/content/366/1565/680.shorthttp://rstb.royalsocietypublishing.org/cgi/doi/10.1098/rstb.2010.0199`.

Roman Huber and Markus Knaden. Egocentric and geocentric navigation during extremely long foraging paths of desert ants. *Journal of Comparative Physiology A: Neuroethology, Sensory, Neural, and Behavioral Physiology*, 201(6):609–616, 2015. ISSN 1432-1351. doi: 10.1007/s00359-015-0998-3.

Brad K. Hulse and Vivek Jayaraman. Mechanisms Underlying the Neural Computation of Head Direction. *Annual Review of Neuroscience*, 43:31–54, 2020. ISSN 1545-4126. doi: 10.1146/annurev-neuro-072116-031516.

Kyobi S. Kakaria and Benjamin L. de Bivort. Ring Attractor Dynamics Emerge from a Spiking Model of the Entire Protocerebral Bridge. *Frontiers in Behavioral Neuroscience*, 11:8, February 2017. ISSN 1662-5153. doi: 10.3389/fnbeh.2017.00008.

DaeEun Kim and John C.T. Hallam. Neural network approach to path integration for homing navigation. In *From Animals to Animats 6*, pages 228—235. MIT Press, 2000.

DaeEun Kim and Jiwon Lee. Path integration mechanism with coarse coding of neurons. *Neural Processing Letters*, 34(3):277–291, December 2011. ISSN 1370-4621. doi: 10.1007/s11063-011-9198-5.

Irene S. Kim and Michael H. Dickinson. Idiothetic Path Integration in the Fruit Fly Drosophila melanogaster. *Current Biology*, 27(15):2227–2238, 2017. ISSN 0960-9822. doi: 10.1016/j.cub.2017.06.026. URL `https://www.sciencedirect.com/science/article/pii/S0960982217307285`.

Sung Soo Kim, Hervé Rouault, Shaul Druckmann, and Vivek Jayaraman. Ring attractor dynamics in the Drosophila central brain. *Science*, 356(6340):849–853, May 2017. ISSN 1095-9203. doi: 10.1126/science.aal4835. URL http://science.sciencemag.org/content/early/2017/05/03/science.aal4835.fullhttp://www.ncbi.nlm.nih.gov/pubmed/28473639.

B L McNaughton, C a Barnes, J L Gerrard, K Gothard, M W Jung, J J Knierim, H Kudrimoti, Y Qin, W E Skaggs, M Suster, and K L Weaver. Deciphering the hippocampal polyglot: the hippocampus as a path integration system. *The Journal of experimental biology*, 199(Pt 1):173–185, 1996. ISSN 0022-0949.

Bruce L. McNaughton, Francesco P. Battaglia, Ole Jensen, Edvard I Moser, and May-Britt Moser. Path integration and the neural basis of the 'cognitive map'. *Nature Reviews Neuroscience*, 7(8): 663–678, August 2006. ISSN 1471-003X. doi: 10.1038/nrn1932. URL http://www.nature.com/articles/nrn1932http://www.nature.com/doifinder/10.1038/nrn1932.

R. Menzel and U. Muller. Learning and memory in honeybees: From behavior to neural substrates. *Annual Review of Neuroscience*, 19:379—404, 1996. ISSN 0147-006X. doi: 10.1146/annurev.ne.19.030196.002115.

M. L. Mittelstaedt and H. Mittelstaedt. Homing by path integration in a mammal. *Naturwissenschaften*, 67(11):566–567, November 1980. ISSN 1432-1904. doi: 10.1007/BF00450672.

M Müller and R Wehner. Path integration in desert ants, Cataglyphis fortis. In *Proceedings of the National Academy of Sciences of the United States of America*, volume 85, pages 5287–5290. National Acad Sciences, 1988. doi: 10.1073/pnas.85.14.5287. URL http://www.pnas.org/content/85/14/5287.short.

Keram Pfeiffer and Uwe Homberg. Organization and Functional Roles of the Central Complex in the Insect Brain. *Annual Review of Entomology*, 59(1):165–184, January 2013. ISSN 0066-4170. doi: 10.1146/annurev-ento-011613-162031.

Paul Pfeiffer, Alexei V Egorov, Franziska Lorenz, Jan-hendrik Schleimer, Andreas Draguhn, and Susanne Schreiber. Clusters of cooperative ion channels enable a membrane-potential-based mechanism for short-term memory. *eLife*, 9:1–27, 2020. ISSN 2050-084X. doi: 10.7554/eLife.49974. URL https://elifesciences.org/articles/49974.

Ioannis Pisokas, Stanley Heinze, and Barbara Webb. The head direction circuit of two insect species. *eLife*, 9:e53985, July 2020. ISSN 2050-084X. doi: 10.7554/eLife.53985.

Ioannis Pisokas, Wolfgang Rössler, Barbara Webb, Jochen Zeil, and Ajay Narendra. Anesthesia disrupts distance, but not direction, of path integration memory. *Current Biology*, 32(2):445–452, 2021. ISSN 0960-9822. doi: 10.1016/j.cub.2021.11.039.

Michael Postlethwaite, Matthias H Hennig, Joern R Steinert, Bruce P Graham, and Ian D Forsythe. Acceleration of ampa receptor kinetics underlies temperature-dependent changes in synaptic strength at the rat calyx of held. *The Journal of Physiology*, 579(1):69–84, 2007.

Joshua I. Raji and Christopher J. Potter. The number of neurons in Drosophila and mosquito brains. *PLOS ONE*, 16(5):e0250381, 2021. doi: 10.1371/journal.pone.0250381.

A. David Redish, Adam N. Elga, and David S. Touretzky. A coupled attractor model of the rodent Head Direction system. *Network: Computation in Neural Systems*, 7(4):671–685, January 1996. ISSN 0954-898X. doi: 10.1088/0954-898X_7_4_004. URL https://www.tandfonline.com/doi/full/10.1088/0954-898X{_}7{_}4{_}004.

Alexei Samsonovich and Bruce L. McNaughton. Path integration and cognitive mapping in a continuous attractor neural network model. *The Journal of neuroscience : the official journal of the Society for Neuroscience*, 17(15):5900–20, 1997. ISSN 0270-6474. URL http://www.jneurosci.org/content/17/15/5900.fullhttp://www.ncbi.nlm.nih.gov/pubmed/9221787.

Johannes D. Seelig and Vivek Jayaraman. Neural dynamics for landmark orientation and angular path integration. *Nature*, 521(7551):186–191, May 2015. ISSN 1476-4687. doi: 10.1038/nature14446.

H S Seung. How the brain keeps the eyes still. *Proceedings of the National Academy of Sciences of the United States of America*, 93(23):13339–44, November 1996. ISSN 0027-8424. URL http://www.ncbi.nlm.nih.gov/pubmed/8917592http://www.pubmedcentral.nih.gov/articlerender.fcgi?artid=PMC24094.

W E Skaggs, J J Knierim, H S Kudrimoti, and B L McNaughton. A model of the neural basis of the rat's sense of direction. *Advances in neural information processing systems*, 7(1984):173–80, 1995. ISSN 1049-5258. URL http://www.ncbi.nlm.nih.gov/pubmed/11539168.

S. Sommer and R. Wehner. The ant's estimation of distance travelled: experiments with desert ants, Cataglyphis fortis. *Journal of Comparative Physiology A: Sensory, Neural, and Behavioral Physiology*, 190(1):1–6, January 2004. ISSN 0340-7594. doi: 10.1007/s00359-003-0465-4.

Thomas Stone, Barbara Webb, Andrea Adden, Nicolai Ben Weddig, Anna Honkanen, Rachel Templin, William Wcislo, Luca Scimeca, Eric Warrant, and Stanley Heinze. An Anatomically Constrained Model for Path Integration in the Bee Brain. *Current Biology*, 27(20):3069–3085, 2017. ISSN 0960-9822. doi: 10.1016/j.cub.2017.08.052. URL https://www.sciencedirect.com/science/article/pii/S0960982217310904.

Ta Shun Su, Wan Ju Lee, Yu Chi Huang, Cheng Te Wang, and Chung Chuan Lo. Coupled symmetric and asymmetric circuits underlying spatial orientation in fruit flies. *Nature Communications*, 8 (1):1–15, December 2017. ISSN 2041-1723. doi: 10.1038/s41467-017-00191-6. URL http://dx.doi.org/10.1038/s41467-017-00191-6www.nature.com/naturecommunications.

Lamont S. Tang, Marie L. Goeritz, Jonathan S. Caplan, Adam L. Taylor, Mehmet Fisek, and Eve Marder. Precise Temperature Compensation of Phase in a Rhythmic Motor Pattern. *PLoS Biology*, 8(8):e1000469, 2010. ISSN 1544-9173. doi: 10.1371/journal.pbio.1000469.

Daniel Turner-Evans, Stephanie Wegener, Hervé Rouault, Romain Franconville, Tanya Wolff, Johannes D Seelig, Shaul Druckmann, and Vivek Jayaraman. Angular velocity integration in a fly heading circuit. *eLife*, 6:2112–2126, May 2017. ISSN 2050-084X. doi: 10.7554/elife.23496. URL http://www.ncbi.nlm.nih.gov/pubmed/28530551http://www.pubmedcentral.nih.gov/articlerender.fcgi?artid=PMC5440168http://elifesciences.org/lookup/doi/10.7554/eLife.23496.

Daniel B Turner-Evans and Vivek Jayaraman. The insect central complex. *Current Biology*, 26 (11):R453–R457, June 2016. ISSN 0960-9822. doi: 10.1016/j.cub.2016.04.006. URL http://linkinghub.elsevier.com/retrieve/pii/S0960982216303232.

Daniel B. Turner-Evans, Kristopher T. Jensen, Saba Ali, Tyler Paterson, Arlo Sheridan, Robert P. Ray, Tanya Wolff, J. Scott Lauritzen, Gerald M. Rubin, Davi D. Bock, and Vivek Jayaraman. The Neuroanatomical Ultrastructure and Function of a Biological Ring Attractor. *Neuron*, 108 (1):145–163, 2020. ISSN 1097-4199. doi: 10.1016/j.neuron.2020.08.006.

R. J. Vickerstaff and E. A. Di Paolo. Evolving neural models of path integration. *Journal of Experimental Biology*, 208(17), 2005. URL http://jeb.biologists.org/content/208/17/3349.full.

Robert J. Vickerstaff and Allen Cheung. Which coordinate system for modelling path integration? *Journal of Theoretical Biology*, 263(2):242–261, 2010. ISSN 0022-5193. doi: 10.1016/j.jtbi.2009.11.021.

M. Volgushev, T. R. Vidyasagar, M. Chistiakova, and U. T. Eysel. Synaptic transmission in the neocortex during reversible cooling. *Neuroscience*, 98(1):9—22, 2000. ISSN 0306-4522. doi: 10.1016/s0306-4522(00)00109-3.

Karl von Frisch. *The dance language and orientation of bees*. Harvard University Press, 1967. ISBN 9780674418776. URL https://discovered.ed.ac.uk/primo-explore/fulldisplay?docid=44UOE{_}ALMA21123598440002466{&}context=L{&}vid=44UOE{_}VU2{&}lang=en{_}US{&}search{_}scope=default{_}scope{&}adaptor=LocalSearchEngine{&}tab=default{_}tab{&}query=any,contains,Thedancelanguageandorienta.

Barbara Webb and Antoine Wystrach. Neural mechanisms of insect navigation. *Current Opinion in Insect Science*, 15:27–39, 2016. ISSN 2214-5745. doi: 10.1016/j.cois.2016.02.011. URL https://www.sciencedirect.com/science/article/pii/S221457451630013X.

Peter T Weir and Michael H Dickinson. Functional divisions for visual processing in the central brain of flying Drosophila. *Proceedings of the National Academy of Sciences of the United States of America*, 112(40):E5523–E5532, October 2015. ISSN 1091-6490. doi: 10.1073/pnas.1514415112. URL http://www.ncbi.nlm.nih.gov/pubmed/26324910http://www.pubmedcentral.nih.gov/articlerender.fcgi?artid=PMC4603480.

Thomas Wittmann and Helmut Schwegler. Path integration - a network model. *Biological Cybernetics*, 73(6):569–575, November 1995. ISSN 0340-1200. doi: 10.1007/BF00199549.

Tanya Wolff and Gerald M. Rubin. Neuroarchitecture of the Drosophila central complex: A catalog of nodulus and asymmetrical body neurons and a revision of the protocerebral bridge catalog. *Journal of Comparative Neurology*, 526(16):2585–2611, August 2018. ISSN 1096-9861. doi: 10.1002/cne.24512.

K Zhang. Representation of spatial orientation by the intrinsic dynamics of the head-direction cell ensemble: a theory. *The Journal of Neuroscience*, 16(6):2112–2126, March 1996. ISSN 0270-6474. doi: 10.1523/jneurosci.16-06-02112.1996. URL http://www.ncbi.nlm.nih.gov/pubmed/8604055.

P. E. Ziegler and R. Wehner. Time-courses of memory decay in vector-based and landmark-based systems of navigation in desert ants, Cataglyphis fortis. *Journal of Comparative Physiology - A Sensory, Neural, and Behavioral Physiology*, 181(1):13–20, June 1997. ISSN 0340-7594. doi: 10.1007/s003590050088.